

High efficiency magneto-optical trap for unstable isotopes

S. Aubin,^{a)} E. Gomez, L. A. Orozco, and G. D. Sprouse

Department of Physics and Astronomy, State University of New York, Stony Brook, New York 11794-3800

(Received 10 March 2003; accepted 25 June 2003)

We have trapped over 250 000 ^{210}Fr in a new on-line high efficiency magneto-optical trap (MOT). We describe the new apparatus and present an overview of high-efficiency MOTs for trapping rare isotopes. These traps depend on three critical components: a dry-film coating, a neutralizer, and the optical trap. We have developed a series of independent tests of the effectiveness of these components, and have used the results to construct our trap. © 2003 American Institute of Physics. [DOI: 10.1063/1.1606093]

I. INTRODUCTION

Rare and artificial isotopes are attractive systems in which to test weak interaction violations of discrete symmetries predicted by the standard model. Experiments in such atoms benefit from larger single atom effects than in more stable species, but still require a large number of atoms to yield more precise measurements of the electroweak interaction and its parameters. For example, the TISOL group at TRIUMF is studying neutrino mixing through β -decay measurements on ^{38m}K (half-life 0.9 s),¹ while Freedman *et al.* are performing similar studies in ^{21}Na (half-life 22 s).² Vieira *et al.* have observed parity violation in the spatial distribution of β -particles in ^{82}Rb (half-life 75 s) at Los Alamos.³ Moi *et al.* at Pisa-Legnaro and our group at Stony Brook are both interested in parity violation in francium (^{210}Fr half-life 3.2 min) through direct Z_0 exchange and the nuclear anapole moment.^{4,5} In the beta-decay experiments unstable isotopes are necessary for high event rates, while in francium the expected per atom parity violating effects are an order of magnitude larger than in other alkali atoms such as cesium.⁶

Precision measurements on trapped atoms benefit from low field, controllable, substrate-free environments and very low temperatures. While many types of traps have been invented, the magneto-optical trap (MOT) is the most commonly used so far and is ideally applicable to alkali atoms. The MOT provides a cold atom source from a simple vapor or a slow atomic beam. An essential component of rare isotope experiments is the trapping of a large fraction of the available atoms. In off-line experiments, the atoms are typically more stable but very rare, and successful high efficiency traps have been constructed for these.^{7,8} In on-line experiments, the unstable isotopes are produced artificially through fission or fusion reactions at very low rates, typically $\sim 10^6$ atoms/s or less. The atoms must be extracted quickly from the production area and trapped efficiently since they are short-lived and few.

We have constructed and designed a high efficiency MOT for francium. We have trapped over 250 000 ^{210}Fr atoms at a single time and have observed average trap sizes of

50 000 atoms for periods of over 5 min. The design is based on a pulsed trapping scheme and can be easily adapted to other species. In this article we detail the production and trapping apparatus, the essential components of the trap, useful diagnostic tests, and our results with francium. The article is divided into seven sections: new apparatus (II), optical trapping (III), the trapping cell (IV), neutralizer studies (V), detection (VI), trapping efficiency (VII), and results (VIII).

II. NEW APPARATUS

The new apparatus (see Fig. 1) follows the general design of our first generation radioactive traps.^{9–11} It features a production chamber, a transport system, and a trapping cell. The main differences from the original system are a 10 m transport beamline, an improved target, and a pulsed high efficiency MOT.

A. Target

We produce francium nuclei, the heaviest of the alkalis, in a heavy ion fusion reaction between an oxygen ion beam and a gold target. The SUNY at Stony Brook Superconducting LINAC provides 1.3 μA of ~ 100 MeV $^{18}\text{O}^{5+}$. The energy of the oxygen beam is sufficient to overcome the inter-nuclear Coulomb barrier and the nuclei fuse. The resulting francium nucleus stabilizes by boiling off excess neutrons. The number of evaporated neutrons is determined by the oxygen beam energy, and consequently different isotopes form at different target depths. While the results reported here are for ^{210}Fr , we can make other isotopes, $^{208-210}\text{Fr}$, by varying the incident beam energy, isotope, and atomic number.¹²

The oxygen beam impacts the target at an angle of 45° . The target consists of a lump of gold melted and flattened onto the end of a 6 mm diameter tungsten rod with a thickness of 0.3 mm (600 mg/cm^2).¹³ While a resistive coils heats the target, the incident beam also provides a considerable amount of heating power ($100\text{ MeV} \times 1.3\ \mu\text{A}$) onto a very small area ($\sim 1\text{ mm}^2$). We monitor the surface temperature of the target with a charge coupled device (CCD) camera with near infrared sensitivity. The thermal imaging allows us to both steer the oxygen beam on the target and keep the beam intensity just below the melting point of the target surface to

^{a)}Electronic mail: seth.aubin@sunysb.edu

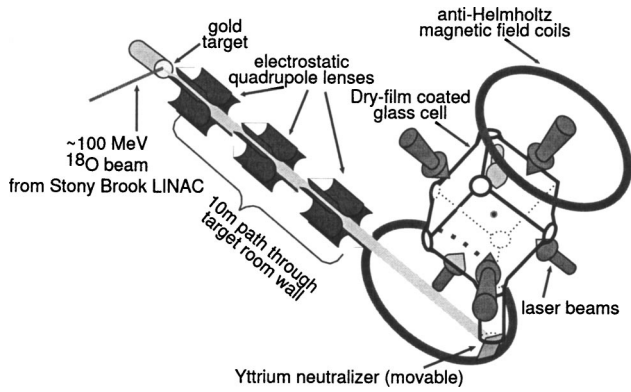


FIG. 1. On-line apparatus for francium production and trapping. The drawing is not to scale.

increase the diffusion of francium to the surface. The target collimator is large enough to allow for some steering of the oxygen beam over the target area. This feature is particularly useful in the event of accidental localized melting and damage to the target surface by an overly intense oxygen beam.

The francium fusion reaction produces many neutrons at about 5 MeV in the target area. At these energies, neutrons pose a significant radiation hazard, limiting target access to remote controlled instruments. In order to work in a neutron-free environment, we remove the francium from the target as an ion and transport it to the trapping room, located 10 m away behind a 1 m thick concrete wall.

With the target just below the melting temperature of gold, the embedded francium diffuses rapidly to the surface and evaporates. The francium desorbs from the target surface as atoms and ions according to the Langmuir–Saha equation:¹⁴

$$\frac{n_+}{n_0} = \frac{\omega_+}{\omega_0} \exp\left(\frac{E_{WF} - E_{IP}}{kT}\right), \quad (1)$$

where n_+/n_0 is the ratio of ions to atoms desorbed, ω_+/ω_0 is the ratio of statistical weights and equals 1/2 for alkali atoms, E_{WF} is the work function of the surface, and E_{IP} is the ionization potential of the desorbed atom. Since for gold E_{WF} is 5.1 eV (see Table I for E_{IP} of francium and rubidium), we have $E_{WF} > E_{IP}$, and consequently the target emits primarily Fr^+ ions. While francium isotopes can be produced in other fusion reactions, we choose to use gold as a target since it is a noble metal, naturally monoisotopic, and provides an ionizing surface for alkali atoms.

B. Transport beamline

Once desorbed from the target surface, we accelerate the francium ions across a 5 keV potential and guide them electrostatically to the trapping room. The electrostatic optics of our transport beamline ensure mass independent transport of all francium isotopes and even other alkalis, such as rubidium, which we use for testing most of our apparatus.⁹ After acceleration, we collimate the ions with an Einzel lens, steer them around a 90° turn with a two step bender, and use a series of steerer plates and quadrupole lenses to direct the ions to the trapping region (see Fig. 2). At the end of the transport beamline, we focus the ions through a collimator onto a neutralizer with a second Einzel lens. A constriction in the beamline before this last Einzel lens allows for differential pumping of the trapping region. At present we can sustain typically 1×10^6 Fr/s to the beamline Faraday cup (silicon detector No. 2 in Fig. 2). We transport ions from the bender Faraday cup (silicon detector No. 1) to the beamline Faraday cup in the trapping room with an efficiency of over 90%.

After collecting francium on the neutralizer for a short time, typically 30 s, we swing the neutralizer up to the trapping cell orifice and heat a 0.13 mm thick yttrium neutralizer to above 1000 K for 1 s with a current of 7 A. Since yttrium has a work function $E_{WF} = 3.1$ eV,¹⁵ almost all the francium is released as atoms [see Eq. (1)]. The francium atoms desorb into the cell where they are trapped by a high efficiency MOT. The neutralizer is designed so as to completely plug the trapping cell orifice.

The francium production rate is too low to align the entire apparatus with it. However, by performing a coarse tuning of the apparatus using rubidium, which has similar electronic properties to francium (see Table I), we can then tune the francium beam by counting its α decays. We spray rubidium from a dispenser onto the target to create an ion source the size of the target. We align the beamline and optimize the trapping setup with the Rb^+ ions. We then fine tune the beamline alignment with francium by removing the neutralizer, and letting the ion beam hit a thin nickel foil in front of silicon detector No. 3 (see Fig. 2). The francium ion beam is aligned once the steady state α -particle rate detected by the silicon detector has been maximized.

The beamline vacuum is maintained at 1×10^{-8} Torr by two 150 l/s ion pumps (Varian StarCell 150) installed at quadrupole lens 3 and after the constriction, a 300 l/s tur-

TABLE I. Atomic and electronic properties of ²¹⁰Fr and ⁸⁵Rb.

	⁸⁵ Rb	²¹⁰ Fr
Ionization potential (Ref. 16)	4.18 eV	4.08 eV
Nuclear spin	5/2	6
Two-level atom saturation intensity	1.6 mW/cm ²	2.7 mW/cm ²
Linewidth of D2 cycling transition	6.06 MHz	7.57 MHz
Wavelength of D2 upper cycling transition	12 816.008 cm ⁻¹	13 923.381(1) cm ⁻¹
Wavelength of D1 repumping transition	12 579.012 cm ⁻¹	12 238.425(1) cm ⁻¹
	5S _{1/2} F=3 → 5P _{3/2} F=4	7S _{1/2} F=13/2 → 7P _{3/2} F=15/2
	5S _{1/2} F=2 → 5P _{1/2} F=3	7S _{1/2} F=11/2 → 7P _{1/2} F=13/2

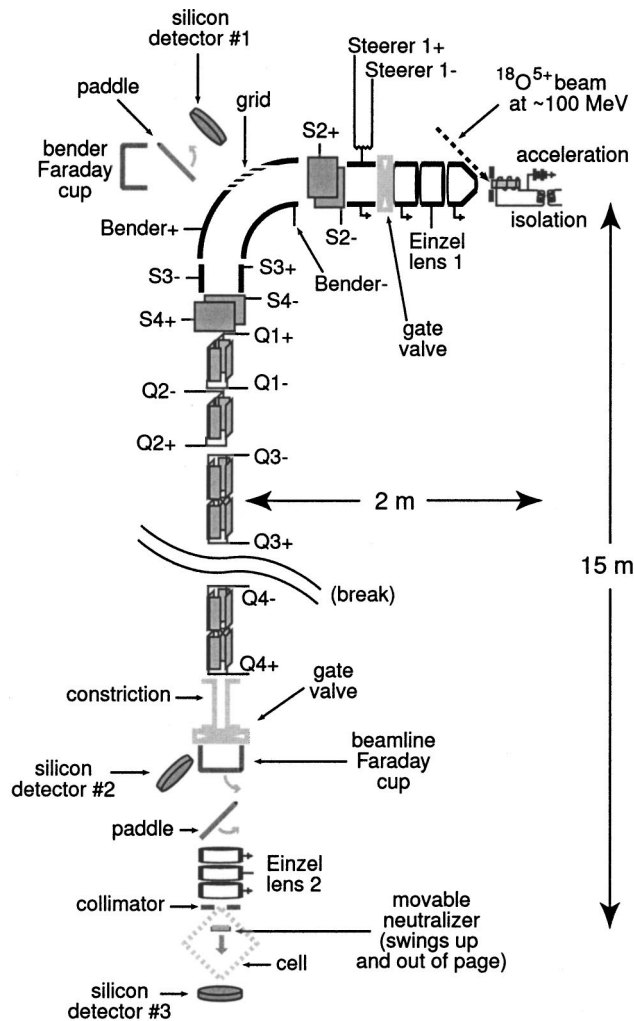


FIG. 2. Schematic of the transport beamline (not to scale). Q denotes a quadrupole lens electrode. S denotes a steering element electrode.

bopump (Varian Navigator) placed immediately after the constriction, and a getter pump (SAES NEG Pump) located at the second Einzel lens. The large number of pumps between Einzel lens 2 and the beamline constriction are important to help maintain a vacuum of 5×10^{-9} Torr in the trapping region. The trapping cell is pumped by a 20 l/s ion pump (Varian StarCell 20) and a small getter pump (SAES CapaciTorr) located directly below it. The target region is pumped by a 330 l/s turbopump (Balzer Pfeiffer TPU 330 U) installed directly underneath it. With a hot target over 1000 K the vacuum is typically better than 1×10^{-7} Torr in the production chamber where oxygen fuses with gold to produce francium.

C. Trapping cell

The cell for the MOT consists of a glass cube, 5 cm on the side, with 1.5 cm in diameter windows at the corners of the cube (see Fig. 1). A glass neck 1.5 cm in diameter connects one of the corners of the cell to a standard 2.75 in. conflat window flange (Larson Electronic Glass). The trap is formed by the intersection of three retro-reflected laser beams with a $1/e$ intensity diameter of 3 cm. These beams consist of both trapping and repumper light. We operate with

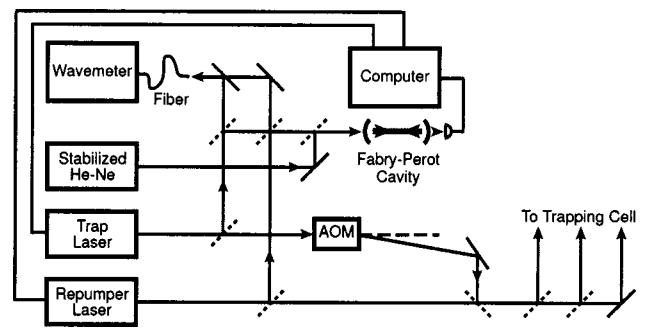


FIG. 3. Schematic of the optical trapping setup.

a typical trapping beam intensity of 18 mW/cm^2 per arm. We overlap a repumper laser over all three arms of the trapping laser. The repumper beams have an intensity of roughly 3 mW/cm^2 and a spatial profile similar to the trapping beams. A current of 25 A running through a pair of 10 cm diameter coils in anti-Helmholtz configuration provides a magnetic field gradient of 6 G/cm.

A Coherent 899-21 provides laser power at 718 nm for trapping on the $7S_{1/2}F = 13/2 \rightarrow 7P_{3/2}F = 15/2$ cycling transition. A second Coherent 899-21 provides light at 817 nm for repumping on the $7S_{1/2}F = 11/2 \rightarrow 7P_{1/2}F_{13/2}$ transition. Due to the absence of francium vapor cells, both these lasers are locked to a stabilized He-Ne laser using a scanning Fabry-Perot cavity.¹⁶ A high accuracy wavemeter (Burleigh 1300) with an uncertainty of $\pm 0.001 \text{ cm}^{-1}$ (30 MHz) provides a coarse frequency reference. We send the trapping light through a single pass acousto-optic modulator (AOM) for fast amplitude modulation and overlap the first diffracted order with the repumper light. The combined beam is then separated into three trapping beams that are sent to the trapping cell (see Fig. 3).

We detect the trapped atoms by imaging their fluorescence onto both a high-speed cooled CCD camera (Roper Scientific, MicroMax 1300YHS-DIF) and a photomultiplier tube (Hamamatsu R636) with a single 1:1 imaging system ($f/3.9$). Optical bandpass filters at 718 nm reduce the background due to room light. We observe the atoms through one of the corner windows of the trapping cell (see Fig. 1).

The design and construction of the target and the transport beamline follow well established techniques,¹⁷ while the high efficiency MOT is a relatively new technology. We dedicate the rest of the article to design considerations and tools needed for constructing a high efficiency MOT and diagnosing its performance. The necessary components of the trapping apparatus are: the optical trap, the trapping cell, the neutralizer, and the detection optics. The first three of these contribute to the trapping efficiency of the apparatus, while the last is necessary for measuring its performance.

III. OPTICAL TRAPPING

The MOT cools and traps atoms that pass through it by dissipating their momentum through the absorption and spontaneous emission of near resonant photons.¹⁸ We can describe the trapping process of an atom from a vapor in the following manner: if an atom enters the trapping region with

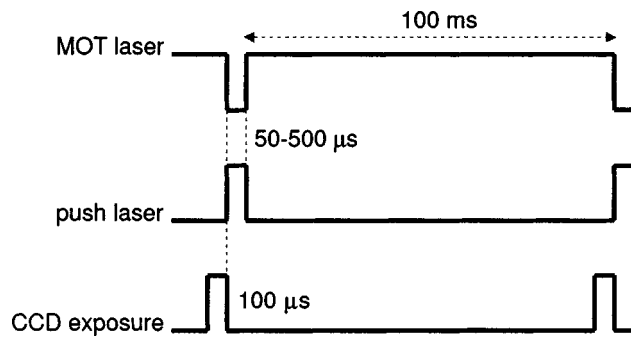


FIG. 4. Summary of the timing sequence for measuring a lower bound for the escape velocity of a MOT (not to scale). The MOT lifetime is over 1 s.

a sufficiently low velocity it will be captured. We can construct a simple model of the trapping process by assuming a uniform capture velocity, the maximum velocity an atom can have and still be trapped, over a characteristic trapping volume.¹⁹ The trapping volume is the effective region over which an atom will be trapped, if inside it with a velocity lower than the capture velocity. The optical trap must be designed to maximize two properties of the MOT in order to capture the largest number of atoms: (1) f_v , the ratio of the trapping volume to the total available volume, and (2) v_c , the capture velocity. While f_v can be estimated from the geometry of the trapping cell and laser beams, determining v_c is more difficult. Moreover, the number atoms trapped from a vapor depends strongly on v_c .

The probability of capturing an atom passing through the trapping volume, $P_1(v_c)$, is given to lowest order in v_c by

$$P_1(v_c) \approx \frac{1}{3} \sqrt{\frac{2}{\pi}} \left(\frac{m}{kT} \right)^{3/2} v_c^3, \quad (2)$$

where we have assumed an atom of mass m taken from a reservoir at temperature T with Maxwell–Boltzmann statistics. The v_c^3 dependence of $P_1(v_c)$ comes from the low-velocity tail of the Maxwell–Boltzmann distribution. While we have assumed a Maxwell–Boltzmann distributed low-velocity tail for atoms desorbed from a dry-film coated surface, we have found no direct measurements in the literature to support or contradict this assumption.

Theoretically, v_c can be calculated from the equations of motion for a two-level atom in a MOT.¹⁸ Numerical integration of the equations shows that the capture velocity depends primarily on the size of the beams (stopping distance) and their intensity (stopping rate). At constant laser power, the optimum operating point depends on the atomic species and the available laser power, but generally favors beams several centimeters in diameter.^{7,20,21}

Capture velocity studies

In order to verify the efficient operation of our MOT, we developed a measuring technique to place a lower bound on v_c . Instead of measuring the capture velocity of our trap, we determine a lower bound on the escape velocity of the trap (i.e., the minimum velocity an atom in the middle of the trap must have in order to leave it), which provides a lower bound for v_c . We proceed as follows (see Fig. 4): With the trapping beams off briefly, we accelerate the trapped atoms

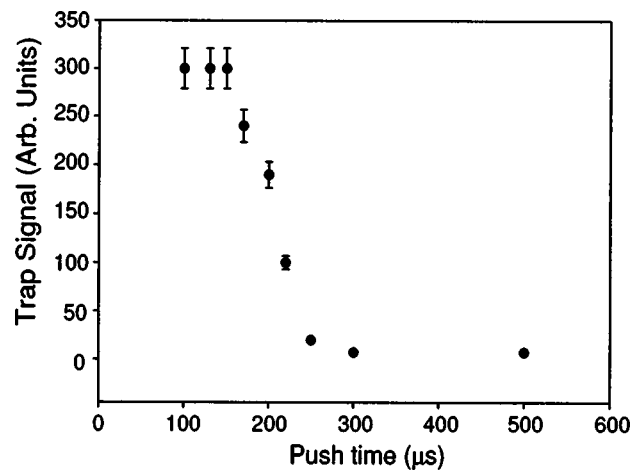


FIG. 5. Plot of the steady state MOT population vs push time in ^{85}Rb . The measurement was done in a different MOT than our high efficiency trap.

with a short, strongly saturating resonant push beam in the horizontal plane. We turn on the trapping beams and measure how many atoms are recaptured. The trapping beams remain on long enough to recapture any pushed atoms, but for a time short compared to the lifetime of the trap to minimize the number of atoms trapped from the background vapor. We extend the cycle by reusing the retrapped atoms, and record the steady state atom number after many cycles as a function of push time (see Fig. 5). The measurement places a lower bound on the escape velocity, since the atoms experience a displacement while being accelerated to their final velocity. For zero initial velocity and uniform acceleration with a push time of $200 \mu\text{s}$ corresponding to a final velocity of 18 m/s as given by the calibration curve of Fig. 6, the atoms are displaced $\sim 2 \text{ mm}$ from the trap center.

For this measurement, we use a MOT formed from elliptical trapping beams ($1.4 \text{ cm} \times 3 \text{ cm}$) in a rectangular trapping cell (inner dimensions: $1.4 \times 1.4 \times 4.0 \text{ cm}^3$) (see Fig. 7). The magnetic field gradient is 15 G/cm . The trapping laser is detuned 17 MHz to the red of the $5S_{1/2} F=3 \rightarrow 5P_{3/2} F=4$

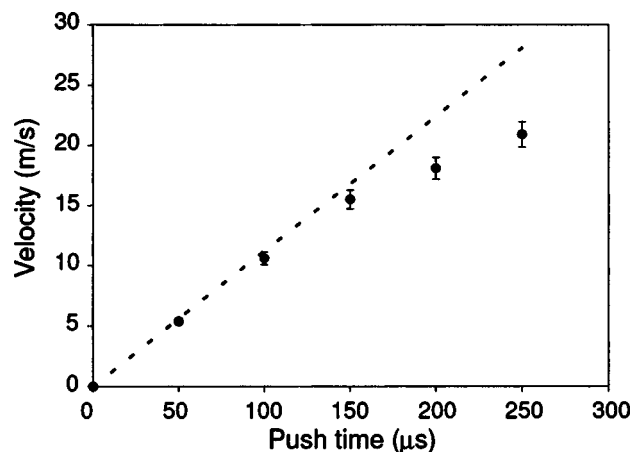


FIG. 6. Calibration curve for converting push time to final velocity. The dotted line represents the theoretical calibration for saturated acceleration. For long push times, the final velocity is smaller than predicted because the atoms are Doppler shifted and the saturation parameter is not infinite.

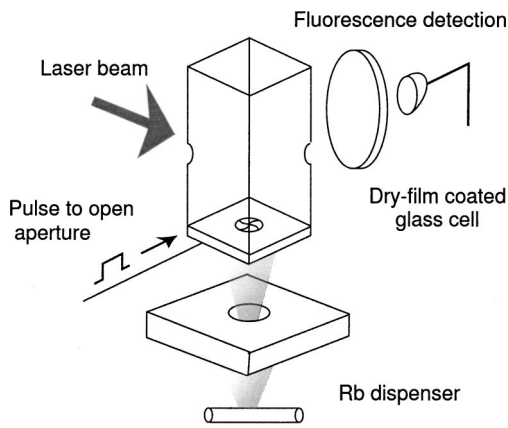


FIG. 7. Experimental setup for testing the dry-film coating of the cell.

cycling transition, while the push beam strongly saturates the same transition.

The final velocity for each push time is obtained in a separate measurement using the CCD camera and a 1:1 imaging system ($f/1.4$). Short exposures are taken immediately after the push and after a few hundred microseconds of flight. From the flight distance measured with the position of the atoms on the images and the time of flight, we calculate the final velocity. In this manner, we construct a calibration curve that converts push time to final velocity (see Fig. 6). The calibration plot agrees well with the theoretical acceleration for a two-level Rb atom in a strongly saturating beam.

From the inflexion point in Fig. 5, we deduce an escape velocity of at least 18 m/s, and $v_c \geq 18$ m/s along the push beam axis. The theoretical capture velocity, obtained from numerical integration of the equations of motion in 1D,¹⁸ together with the experimental magnetic field gradient and laser beam detuning, intensity, and diameter is consistent with this lower bound.

IV. THE TRAPPING CELL

The single pass trapping efficiency, P_1 , is quite small, a typical value for francium is $P_1 = 10^{-5}$. In our experimental setup, we have increased the overall trapping efficiency by forcing the atoms through the trapping region multiple times and rethermalizing them on the cell walls on each pass. The trapping efficiency depends on the average number of bounces, N_{bounces} , the atoms make inside the trapping cell. A simple analysis of the probabilities yields the trapping efficiency, $P_{\text{cell}}(v_c)$, for atoms inside the cell:

$$P_{\text{cell}}(v_c) = \frac{f_v P_1(v_c)}{1 - \left(1 - \frac{1}{N_{\text{bounces}}}\right) [1 - f_v P_1(v_c)]}, \quad (3)$$

f_v is the ratio of the trapping volume to the total cell volume, and $P_1(v_c)$ is the probability to trap an atom as it passes through the trapping volume [see Eq. (1)]. In the limit of $f_v P_1(v_c) \ll 1/N_{\text{bounces}} \ll 1$, the equation becomes proportional to N_{bounces} :

$$P_{\text{cell}}(v_c) \approx N_{\text{bounces}} f_v P_1(v_c). \quad (4)$$

N_{bounces} depends on the cell wall “stickiness” and cell geometry, and by controlling these we can increase P_{cell} .

A. Dry-film coatings

Francium and rubidium are alkalis and bond to most materials by sharing their single valence electron; in other words, they are quite sticky. Research on optical pumping and polarized alkali vapor targets identified silane based dry-films as coatings on which alkalis are physisorbed but rarely chemisorbed.²² A polarizable atom is physisorbed when it is held to the surface by its own image charge; this is a van der Waal interaction.²³ An atom is chemisorbed when it is removed permanently by forming a chemical bond with a surface. After consulting several studies^{22–24} of dry-film coatings we selected the silane-based SC-77 (mixture of dimethyldichlorosilane and methyltrichlorosilane²⁵) and an afterwash of methyltrimethoxysilane. We prepare and coat our trapping cell using the procedure developed by Fedchak *et al.*²⁴ In principle, the dry-film minimizes the chemisorption of alkalis, while also rethermalizing the velocity distribution of the atoms with a room temperature reservoir before being released back into the cell.

B. Cell geometry

In the limit of no chemisorption by the dry-film, the exit holes area in the cell determines N_{bounces} . In this case,

$$N_{\text{bounces}} = \alpha \frac{S_{\text{cell}}}{S_{\text{exit}}}, \quad (5)$$

where α is a factor of order unity that depends on the cell geometry, S_{cell} is the total internal area of the cell, and S_{exit} is the surface area of the entrance and exit holes of the cell. For example, in the cell used for the capture velocity measurements, $\alpha = 1.6$ as determined by the Monte Carlo simulation described in the next section. In order to maximize N_{bounces} , we must increase S_{cell} and decrease S_{exit} . In general, exit holes must exist because the atoms must be introduced into the trapping cell. In our final apparatus (see Fig. 1), we have eliminated the exit holes by plugging the entrance hole with the neutralizer, while simultaneously dispensing the atoms into the cell. With this design, the number of bounces is limited by the quality of the dry-film coating, how well the neutralizer closes the cell, and the efficiency of the neutralizer.

C. Apparatus for testing the number of bounces

High trapping efficiency requires that the dry-film coating keep physisorption sticking time and chemisorption to a minimum. Unfortunately, it is our experience and that of others²⁴ that the application of dry-film coatings is not consistently successful. A test of the coating quality provides a clear indication of the cell’s contribution to the trapping efficiency. We have developed a test of the coating quality in which we measure the average time, τ_{exit} , that an atom spends bouncing around inside the cell before exiting. By comparing τ_{exit} to a Monte Carlo simulation of the test, we can obtain the N_{bounces} for a perfectly coated cell. In our

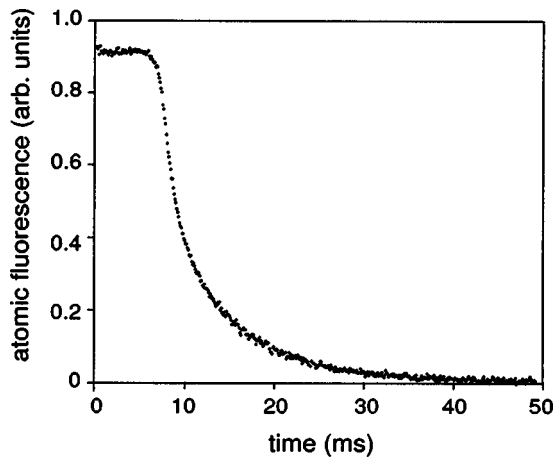


FIG. 8. Fluorescence decay in a coated cell. An exponential fit of the decay gives a characteristic decay time of 6.6 ms ± 1%. A Monte Carlo simulation of the measurement predicts $\tau_{\text{exit}} = 5.2$ ms and an average of 100 bounces.

simulations, the atoms follow Newtonian trajectories inside the cell. When the atoms impact a cell wall, they are reemitted with a cosine distribution and a rethermalized velocity distribution. The atoms do not interact with each other. If the atoms are chemisorbed after only a few bounces, then the measured τ_{exit} will be smaller than its Monte Carlo value. If the atoms have a significant physisorption sticking time, then the measured τ_{exit} will be larger than its Monte Carlo value. We measure τ_{exit} by directing a rubidium atomic beam into the cell through an exit hole and observing the decay of fluorescence from a laser probe when the atomic beam is chopped (see Fig. 7). The cell used for this measurement has exit holes and is the same one used for the capture velocity studies. In our final version of the apparatus, the trapping cell does not have any exit holes. We use a shutter (Uniblitz VS14S1T0) to chop the 4 mm atomic beam with a turn-off time less than 0.5 ms. We detune the laser probe 92 MHz to the red of the $5S_{1/2} F=3 \rightarrow 5P_{3/2} F=4$ in order to preferentially excite atoms in the vapor that are bouncing around inside the cell and not those in the atomic beam. For no optical depumping to the lower hyperfine ground state, the decay of the fluorescence of the atoms inside the cell is exponential with characteristic time τ_{exit} (see Figs. 8 and 9).

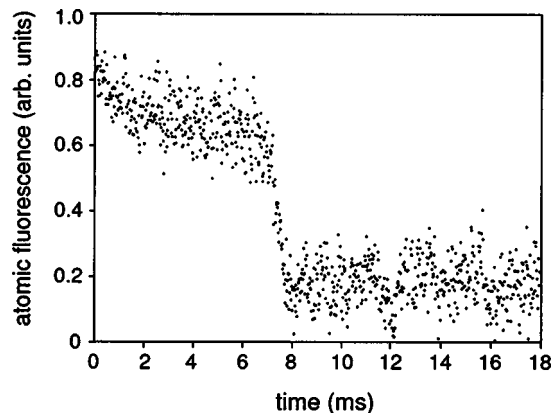


FIG. 9. Fluorescence decay in an uncoated cell. The signal-to-noise ratio in this measurement is lower than in Fig. 8 because there are fewer atoms in the vapor to scatter the probe laser since $N_{\text{bounces}} \approx 1$.

The above method is similar to that used by Stephens *et al.*,²³ but uses a fast shutter and an atomic beam for probing shorter time scales.

We construct a more realistic model of the atoms bouncing around inside the trapping cell by including the physisorption sticking time, τ_s , and chemisorption. In this case, the decay of the fluorescence in Fig. 8 is actually a sum of two exponentials in which the lifetimes are both functions of the average exit time (assuming zero sticking time on the cell walls) and the physisorption sticking time, τ_s . For convenience, the chemisorption probability is included in the average exit time. In the limit of short sticking time, $\tau_{\text{exit}} \gg \tau_s N_{\text{bounces}}$, the decay of fluorescence follows a single exponential. From our data, we find $0 \leq \tau_s \leq 14 \mu\text{s}$, if we assume no optical depumping to the lower hyperfine ground state and no chemisorption.

With the τ_{exit} coating test, we have also been able to verify the importance of curing the coating with rubidium before obtaining satisfactory performance, as well as its degradation with heat, and its deterioration in the presence of commercially available yttrium, a popular neutralizer material.

V. NEUTRALIZER STUDIES

The purpose of the neutralizer is to catch the transported ions and release them into the trapping cell as atoms. We perform these three steps with a cold metal foil into which the ion beam is implanted and then heated to release the ions as atoms. At 5 KeV, the francium ions are embedded about 50 Å deep. Because francium is an alkali, some of it bonds to the neutralizer. The free francium performs a random walk inside the neutralizer foil, with a diffusion time determined by the temperature. Eventually the atoms reach the surface where they desorb with a rate determined by the temperature. The entire process is governed by the rate equation:

$$\frac{d}{dt}N = \xi(T)\rho - \frac{N}{\tau(T)}, \tag{6}$$

where N is the free francium population on the neutralizer, ξ is the fraction of francium atoms that remain free inside the neutralizer, ρ is the francium ion current, and τ is the diffusion time of embedded francium out of the neutralizer.

For high efficiency trapping, we choose a neutralizer material such that $\xi \sim 1$ and $\tau \sim 1$ s. Ideally, the neutralizer will also have a low operating temperature to minimize heat-induced degradation of the dry-film coating. According to Eq. (1), the work function of the surface, E_{WF} must be less than the ionization potential, E_{IP} , of the embedded atom. In the case of francium, yttrium, zirconium, and thoriated tungsten among others possess these characteristics.

We have measurements of both ξ and τ with a francium ion beam on a zirconium neutralizer. We accumulate francium on the neutralizer for 300 s, measure the embedded francium population, heat the neutralizer, and remeasure the embedded francium population after the neutralizer has cooled. The francium population is measured by rotating the neutralizer towards a silicon detector that measures the francium α -decay rate (see Fig. 10). The neutralizer is heated

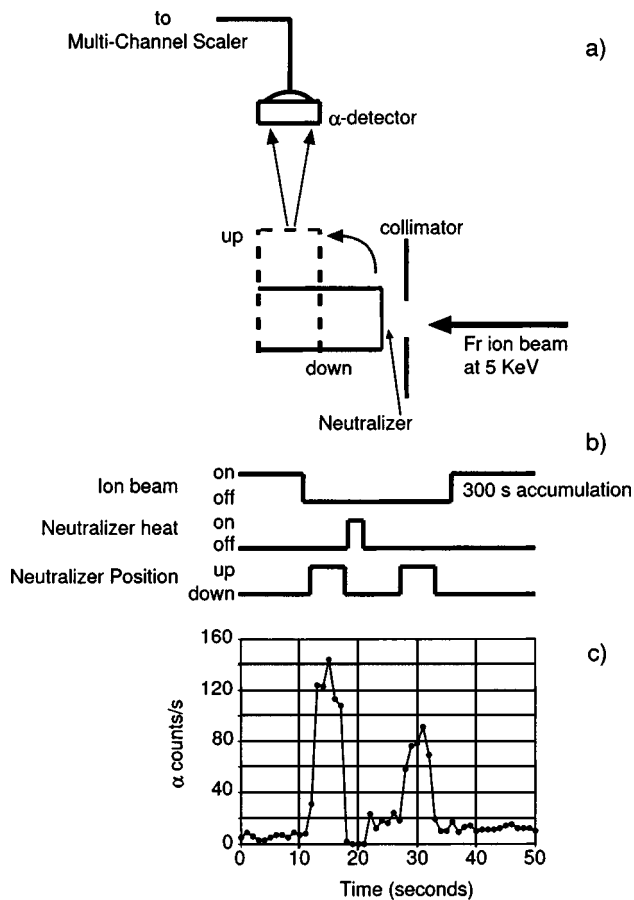


FIG. 10. Neutralizer performance test: (a) Experimental setup, (b) timing scheme, and (c) sample data. In the case of no heat applied to the neutralizer, the second peak shows no decrease from the first.

when pointed away from the α -detector for two reasons: (1) we want to avoid spurious counts from francium which could be deposited on the front surface of the detector, and (2) photons from the heated neutralizer can interfere with detector operation.

By comparing the rate before and after heating, we can determine ξ and τ without measuring absolute populations. The data (see Fig. 11) indicate that $\xi = 0.52 \pm 6\%$ and τ

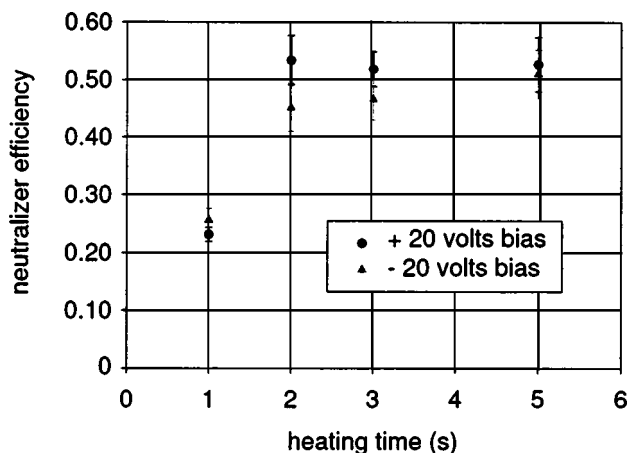


FIG. 11. Neutralizer efficiency of zirconium as a function of heating time. We extract an upper bound on the diffusion time τ , since the neutralizer thermalization time is unknown.

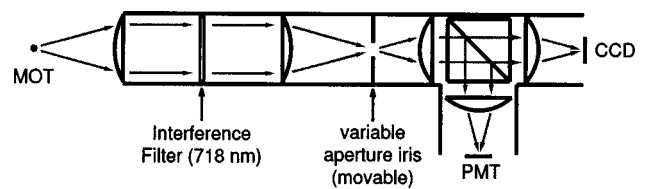


FIG. 12. Sketch of imaging system for detecting MOT fluorescence.

≤ 2 s for $T = 1150 \text{ K} \pm 150 \text{ K}$. Furthermore, above this temperature we see no increase in the neutralizer efficiency. The pulsed nature of the experiment and limited optical access to the neutralizer limit the precision with which we can measure the temperature. The background surrounding the second peak is due to decays from desorbed francium in the vacuum chamber. This background decays to a negligible amount during the 300 s accumulation. Thermal photons render the detector unresponsive while the neutralizer is heated, despite being pointed away. The similarity of the data (see Fig. 11), with the neutralizer biased positively and negatively with respect to the collimator, indicates that francium desorbs primarily as a neutral.

While we have presented results for a zirconium neutralizer, currently we are trapping with a yttrium neutralizer. Commercial yttrium is known to degrade the quality of the SC-77 dry-film coating,²⁶ however, it has neutralized francium reliably in the past.¹¹

VI. DETECTION

We measure the MOT population by imaging the trapping light scattered by the trapped atoms. At the output of our imaging system we direct the light onto both a high resolution CCD camera and a photomultiplier tube. This configuration allows us to center a movable aperture on the MOT and significantly reduce the background scatter detected (see Fig. 12). Even with the aperture, our signal-to-noise ratio remains limited by background intensity fluctuations. These fluctuations are mainly technical and are caused by variations in the laser intensity and pointing stability. We reduce the trap laser intensity fluctuations by a factor of 5 by feeding back on the intensity of the +1 diffracted order out the AOM (see Fig. 3) through the amplitude of the rf signal that powers it.

On the photomultiplier tube (PMT), we filter out the background fluctuations by using two lock-in amplifier techniques: (1) We dither the trapping laser frequency by no more than γ , the linewidth of the cycling transition, or (2) we dither the repumper laser frequency by several hundred megahertz. We measure the modulation in the trap fluorescence recorded by the PMT at the dither frequency with a lock-in amplifier, reducing the effect of the low frequency intensity fluctuations on our background signal.

On the camera, we reduce the effect of intensity fluctuations by measuring variations in the background of the images in real time and correcting for these on the integrated power. The camera signal contains trap laser intensity variations as well as CCD read noise. We determine the MOT population by measuring the background subtracted integrated power in a region of interest (ROI) of the CCD chip.

The rest of the chip is used to measure the background fluctuations in real time with the imaging aperture fully open: all the pixels outside the ROI are compared to their background values by fitting the intensity changes linearly. The results of the fit are then used to estimate the change in the background of the ROI. This real-time correction scheme reduces measured noise by a factor of 20 or better when the ROI is much smaller (~25% or less) than the total CCD chip. We calculate the MOT population from the light collection efficiency of our imaging system, the camera quantum efficiency, and the scattering rate of a ^{210}Fr atom in a laser light field with the detuning from resonance and total intensity of our MOT trapping beams. We calculate the scattering rate using a two-level atom with a saturation intensity that takes into account all the magnetic sublevels of the trapping transition. This method provides an estimate of the MOT population accurate to within a factor of 2.

The camera typically has a signal-to-noise at least twice that of the PMT. For optimum performance, we operate the camera CCD on a 1.6 s duty cycle with the CCD chip exposed over 60% of the time. The ultimate sensitivity of the camera is better than $80 \text{ atoms} \times \text{Hz}^{1/2}$.

VII. TRAPPING EFFICIENCY

The total trapping efficiency P_{trap} may be calculated from the efficiency of the neutralizer, η_n , the number of bounces of the trapping cell, N_{bounces} , and the single pass trapping efficiency of the optical trap, $f_v P_1(v_c)$:

$$P_{\text{trap}} = \eta_n P_{\text{cell}}(v_c) = \frac{\eta_n f_v P_1(v_c)}{1 - \left(1 - \frac{1}{N_{\text{bounces}}}\right) [1 - f_v P_1(v_c)]}, \quad (7)$$

where we have assumed that the neutralizer does not affect the dry-film coating. In the case of a yttrium neutralizer this is not the case.

Equation (7) shows us how to maximize the trapping efficiency. The efficiency is maximized when the capture velocity, the number of bounces, the neutralizer efficiency, and the trap volume to cell volume ratio are all as large as possible. As we and others have found,^{7,21,27,28} these quantities are optimized by using large high intensity trapping beams, a dry-film coated trapping cell with small entrance and exit holes, a carefully selected neutralizer, and a trapping cell the size of the trapping beams.

Our trapping cell has many features of other high efficiency MOTs (similar beam sizes, neutralizers, and trapping volume-to-cell volume ratios). It differs from that of others,²⁹ in that by using a pulsed system the entrance and exit holes have been effectively eliminated. The number of bounces depends primarily on the quality of the dry-film coating.

Trapping efficiency measurements

Experimentally, we can determine the trapping efficiency with measurements of the ion beam current, ρ , and the MOT loading rate R :

$$P_{\text{trap}} = \frac{R}{\rho} \quad (8)$$

with

$$R = \frac{N_{\text{MOT}}}{\tau_{\text{MOT}}}, \quad (9)$$

where N_{MOT} is the steady state MOT population and τ_{MOT} is the MOT lifetime.¹⁹ Using this method, we have measured our francium trapping efficiency to be $P_{\text{trap}} = 1.2_{-0.75}^{+1.5} \times 10^{-2}$. We determine the MOT population from the fluorescence of the cold atomic cloud. In the case of francium, the ion current is too low to accurately measure electrically. We infer the $^{210}\text{Fr}^+$ flux from the change in α -particle rate detected at silicon detector No. 3 (see Fig. 2) when the neutralizer is lifted to the trapping cell to dispense the accumulated francium.

The all-optical trapping efficiency, P_{cell} , can also be measured experimentally. We determine P_{cell} the same way we measure P_{trap} but with a calibrated source of neutrals. The source of neutral atoms can be either an atomic beam or the atoms in the trap themselves.

For an atomic beam of neutral current ρ_{neutral} , the measurement is identical to the one described above with an ion beam, but with the neutralizer removed. In this case, we determine P_{cell} with a similar formula:

$$P_{\text{cell}} = \frac{R}{\rho_{\text{neutral}}}. \quad (10)$$

This method eliminates the neutralizer from the trapping process, and is a good way of testing its performance indirectly.

If the trapping efficiency is high, the atoms in the trap can be used as a calibrated source of neutrals. The trap is loaded with many atoms from a source of neutrals, such as a neutralizer, that is then rapidly turned off. Before the trap population, N_i , has leaked out of trap, but after the untrapped atoms have left the cell, the trap laser is turned off and a probe beam pushes the MOT atoms onto the cell walls. The trap laser is then turned on again, and the number of atoms in the trap, N_f , recorded. The all-optical trapping efficiency is given by

$$P_{\text{cell}} = \frac{N_f}{N_i}. \quad (11)$$

This last method, similar to one employed by Wieman and coworkers,²⁰ has the advantage that it is independent of how the trap population is determined. Any uncertainties in the scattering rates of the trapped atoms, the collection efficiency of the imaging system, or the quantum efficiency of the detector cancel out. It has the disadvantage that N_f may be hard to measure if P_{cell} is small. Care must also be taken to ensure that N_f is measured with a trap population below the saturation density of the MOT. We measure the all-optical trapping efficiency of our MOT in ^{85}Rb with this method. Figure 13 shows the MOT population before and after the application of the push beam. The trapping beams are off while the atoms are pushed. Using this method in an optimized trap, we measure $P_{\text{cell}} = 1.8 \pm 0.4 \times 10^{-2}$. The measurement is a lower bound on the all-optical trapping efficiency, since the exit hole of the cell is not sealed by a hot neutralizer to reflect escaping atoms when the push beam is applied.

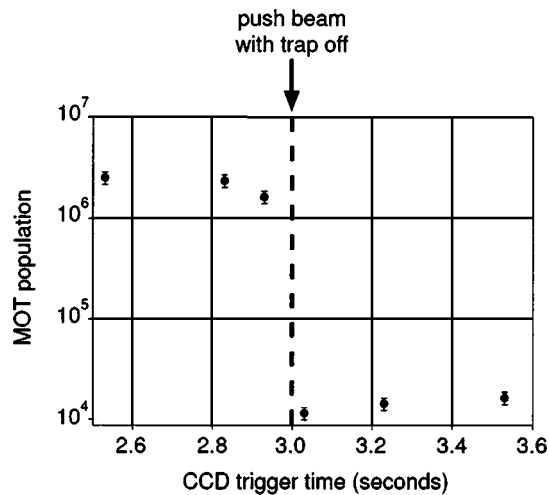


FIG. 13. Trap population before and after laser push. The trap is loaded at $t=0$ s. The neutralizer is turned off and removed at $t=1$ s. The measurement was performed with ^{85}Rb and a 5 ms strongly saturating push beam. Trap population from background vapor was below the sensitivity of the measurement. The error bars on the data points do not include a factor of 2 systematic uncertainty in the MOT population.

VIII. RESULTS

The new apparatus optimizes the trapping efficiency given by Eq. 7: We neutralize efficiently with yttrium, obtain a large trapping volume-to-cell volume ratio by using a cell with the same dimensions as the trapping beams, optimize the capture velocity with large high power laser beams, and maximize the number of bounces by plugging all the exit holes during the trapping process.

We use a pulsed trapping scheme in which we accumulate francium ions on a neutralizer for 32 s and then release them as atoms into the MOT in a 1 s burst. Keeping the cell exit open, while francium accumulates on the neutralizer, improves the vacuum inside the cell. For $3.6 \pm 0.8 \times 10^5$ $^{210}\text{Fr}^+/\text{s}$ incident on the neutralizer, we obtain an average trap population of 50 000 atoms with an average peak population of 1.4×10^5 (see Fig. 14). The downward spike visible in the middle of each cycle in Fig. 14 corresponds to a short pulse of a third off resonant laser that does not affect the MOT performance. When we increase the accumulation period to 3 min, the trap population peaks at 280 000 atoms

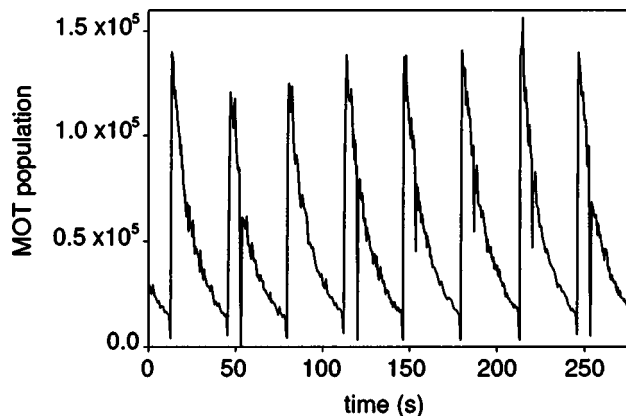


FIG. 14. Plot of francium population in MOT vs time for 32 s of accumulation and a 1 s release.

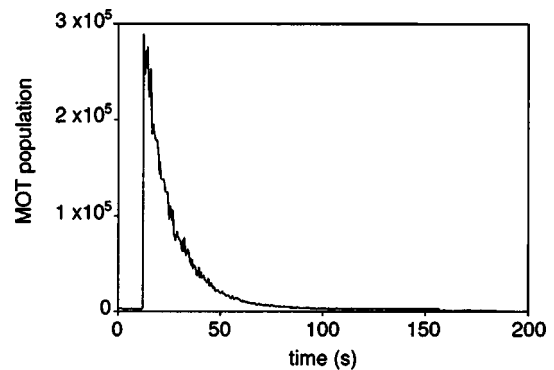


FIG. 15. Plot of francium population in MOT vs time for 170 s of accumulation.

(see Fig. 15). For a background vacuum pressure of 5×10^{-9} as measured by an ion pump current, the trap has a lifetime of 13 s.

The performance of the trap depends strongly on how the neutralizer is heated. We determine experimentally the optimal temperature and heating time of the neutralizer, since the MOT population is a function of both the background pressure in the trapping cell and the number of dispensed francium. While a hot neutralizer releases the francium more quickly and efficiently, it also contributes significantly to the background pressure. This effect is visible in Fig. 14: immediately before the beginning of each MOT loading, the residual trap population vanishes rapidly as the neutralizer heats up. We find that the MOT population is largest when the heating time is limited to 1 s. The temperature is not constant during this time, making its determination difficult. We estimate the optimal temperature (after 1 s of heating) to be at least 1000 K.

We have made a first measurement of the temperature of the ^{210}Fr in our MOT by ballistic expansion of the cold atomic cloud. We turn off the MOT trapping beams for a variable amount of time (3–7 ms) and allow the cold atomic cloud to expand. Immediately after the expansion, we turn the trapping beams back on and take a 1 ms exposure image of the cloud fluorescence to measure its size (see Fig. 16). We estimate that the magneto-optical trapping force modifies

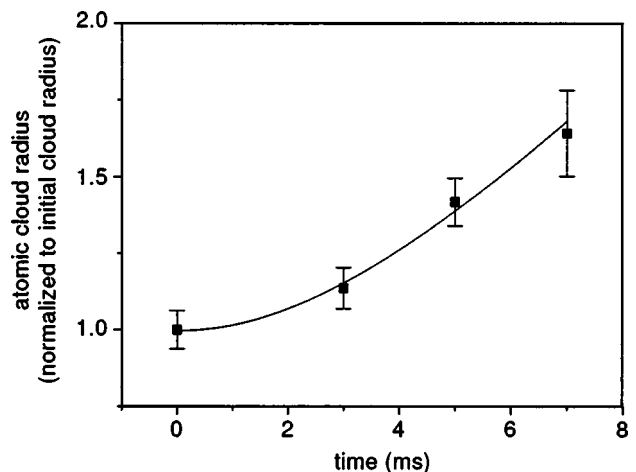


FIG. 16. Plot of the horizontal radius of the atomic cloud as a function of the time the trapping laser is off.

the size of the cold atomic cloud by less than 7% during the course of the exposure. We extract a measurement of the temperature by fitting the data to the expected expansion of a finite size atomic cloud with Maxwell-Boltzmann statistics (solid line in Fig. 16). Difficulty in accurately focusing the image of the MOT on our CCD limits an absolute measurement of the atomic cloud radius. We calculate a temperature of 75 μ K from the expansion rate of the ^{210}Fr cloud, accurate to within a factor of 1.5.

IX. OUTLOOK

In summary, we have constructed a high efficiency trap for francium. We have also developed a series of diagnostic tests of the performance of the trap and its essential components. The design is easily adaptable to other unstable atoms with half-lives longer than 10 s. We expect to improve our trapping efficiency further with other neutralizer materials such as zirconium or thoriated tungsten. From the peak trap sizes of Fig. 14, we anticipate accumulating over 10^6 atoms in steady state by transferring the atoms to a second optical trap that is not pressure limited. This second trap will be in a separate chamber for further physics studies.

ACKNOWLEDGMENTS

Work supported by NSF. E. G. acknowledges support from CONACYT. The authors thank K. Gulyuz, B. Gutshow, R. Lefferts, and J. Sell for maintaining the operation of the Stony Brook LINAC during the francium trapping measurements, as well as A. Lipski for preparing the targets.

¹M. Trinczek, A. Gorelov, D. Melconian, W. P. Alford, D. Asgeirsson, D. Ashery, J. A. Behr, P. G. Bricault, J. M. D'Auria, J. Deutsch, J. Dilling, M. Dombisky, P. Dubé, S. Eaton, J. Fingler, U. Giesen, S. Gu, O. Häusser, K. P. Jackson, B. Lee, J. H. Schmid, T. J. Stocki, T. B. Swanson, and W. Wong, *Phys. Rev. Lett.* **90**, 012501 (2003).

²Z.-T. Lu, C. J. Bowers, S. J. Freedman, B. K. Fujikawa, J. L. Mortara, and S. Q. Shang, *Phys. Rev. Lett.* **72**, 3791 (1994).

³S. G. Crane, S. J. Brice, A. Goldschmidt, R. Guckert, A. Hime, J. J. Kitten, D. J. Vieira, and X. Zhao, *Phys. Rev. Lett.* **86**, 2967 (2001).

⁴G. D. Sprouse and L. A. Orozco, *Annu. Rev. Nucl. Part. Sci.* **47**, 429 (1997).

⁵See, for example, *Trapped Particles and Fundamental Physics, Les Houches 2000*, edited by S. N. Atutov, R. Calabrese, and L. Moi (Kluwer, Amsterdam, 2002), p. 125.

⁶V. A. Dzuba, V. V. Flambaum, and O. P. Sushkov, *Phys. Rev. A* **51**, 3454 (1995).

⁷Z.-T. Lu, K. L. Corwin, K. R. Vogel, C. E. Wieman, T. P. Dinneen, J. Maddi, and H. Gould, *Phys. Rev. Lett.* **79**, 994 (1997).

⁸C. Y. Chen, Y. M. Li, K. Bailey, T. P. O'Connor, L. Young, and Z.-T. Lu, *Science* **286**, 1139 (1999).

⁹J. A. Behr, S. B. Cahn, S. B. Dutta, A. Ghosh, G. Gwinner, C. H. Holbrow, L. A. Orozco, G. D. Sprouse, J. Urayama, and F. Xu, *Nucl. Instrum. Methods Phys. Res. A* **351**, 256 (1994).

¹⁰G. Gwinner, J. A. Behr, S. B. Cahn, A. Ghosh, L. A. Orozco, G. D. Sprouse, and F. Xu, *Phys. Rev. Lett.* **72**, 3795 (1994).

¹¹J. E. Simsarian, A. Ghosh, G. Gwinner, L. A. Orozco, G. D. Sprouse, and P. A. Voytas, *Phys. Rev. Lett.* **76**, 3522 (1996).

¹²J. S. Grossman, L. A. Orozco, M. R. Pearson, J. E. Simsarian, G. D. Sprouse, and W. Z. Zhao, *Phys. Rev. Lett.* **83**, 935 (1999).

¹³A. R. Lipski and M. R. Pearson, *Nucl. Instrum. Methods Phys. Res. A* **480**, 156 (2002).

¹⁴T. Dinneen, A. Ghiorso, and H. Gould, *Rev. Sci. Instrum.* **67**, 752 (1996).

¹⁵*CRC Handbook of Chemistry and Physics*, 71st ed., edited by D. R. Lide (CRC, Boca Raton, FL, 1990).

¹⁶W. Z. Zhao, J. E. Simsarian, L. A. Orozco, and G. D. Sprouse, *Rev. Sci. Instrum.* **69**, 3737 (1998).

¹⁷See, for example, A. I. Pikin, C. A. Morgan, E. W. Bell, L. P. Ratliff, D. A. Church, and J. D. Gillaspay, *Rev. Sci. Instrum.* **67**, 2528 (1996).

¹⁸H. J. Metcalf and P. van der Straten, *Laser Cooling and Trapping* (Springer, Berlin, 1999).

¹⁹C. Monroe, W. Swann, H. Robinson, and C. Wieman, *Phys. Rev. Lett.* **65**, 1571 (1990).

²⁰M. Stephens and C. Wieman, *Phys. Rev. Lett.* **72**, 3787 (1994).

²¹K. E. Gibble, S. Kasapi, and S. Chu, *Opt. Lett.* **17**, 526 (1992).

²²D. R. Swenson and L. W. Anderson, *Nucl. Instrum. Methods Phys. Res. B* **29**, 627 (1988).

²³M. Stephens, R. Rhodes, and C. Wieman, *J. Appl. Phys.* **76**, 3479 (1994).

²⁴J. A. Fedchak, P. Cabauy, W. J. Cummings, C. E. Jones, and R. S. Kowalczyk, *Nucl. Instrum. Methods Phys. Res. A* **391**, 405 (1997).

²⁵Silar Laboratories, Scotia, NY 12303, tel: (518) 372-5691.

²⁶S. G. Crane, X. Zhao, W. Taylor, and D. J. Vieira, *Phys. Rev. A* **62**, 011402 (2000).

²⁷R. Guckert, X. Zhao, S. G. Crane, A. Hime, W. A. Taylor, D. Tupa, D. J. Vieira, and H. Wollnik, *Phys. Rev. A* **58**, R1637 (1998).

²⁸J. A. Behr, A. Gorelov, T. Swanson, O. Husser, K. P. Jackson, M. Trinczek, U. Giesen, J. M. D'Auria, R. Hardy, T. Wilson, P. Chobotov, F. Leblond, L. Buchmann, M. Dombisky, C. D. P. Levy, G. Roy, B. A. Brown, and J. Dilling, *Phys. Rev. Lett.* **79**, 375 (1997).

²⁹M. D. DiRosa, S. G. Crane, J. J. Kitten, W. A. Taylor, D. J. Vieira, and X. Zhao, *Proc. SPIE* **4634**, 34 (2002).